Ultrasound in Med. & Biol., Vol. 26, No. 2, pp. 263–272, 2000

0301-5629/00/$–see front matter

PII S0301-5629(99)00130-1

● *Original Contribution*

RECONSTRUCTION AND VISUALIZATION OF IRREGULARLY SAMPLED THREE- AND FOUR-DIMENSIONAL ULTRASOUND DATA FOR CEREBROVASCULAR APPLICATIONS

STEPHEN MEAIRS, JENS BEYER and MICHAEL HENNERICI
Department of Neurology, University of Heidelberg, Klinikum Mannheim Mannheim, Germany

(*Received* 1 *April* 1999; *in final form* 16 *August* 1999)

Abstract—Although recent studies have demonstrated the potential value of compounded data for improvement in signal-to–noise ratio and speckle contrast for three-dimensional (3-D) ultrasonography, clinical applications are lacking. We investigated the potential of six degrees-of–freedom (6-DOF) scanhead position and orientation measurement (POM) devices for registration of *in vivo* multiplanar, irregularly sampled ultrasound (US) images to a regular 3-D volume space. The results demonstrate that accurate spatial and temporal registration of four-dimensional (4-D) US data can be achieved using a 6-DOF scanhead tracking system. For reconstruction of arbitrary, irregularly sampled US data, we introduce a technique based upon a weighted, ellipsoid Gaussian convolution kernel. Volume renderings of 3-D and 4-D compounded *in vivo* US data are presented. The results, although restricted to the field of cerebrovascular disease, will be of value to other applications of 3-D sonography, particularly those in which compounding of data through irregular sampling may provide superior information on tissue or vessel structure. © 2000 World Federation for Ultrasound in Medicine & Biology.

Key Words: **Three-dimensional ultrasound imaging, Registration, Calibration, Compound data reconstruction, Irregularly sampled ultrasound data, Visualization, Cerebrovascular ultrasound.**

INTRODUCTION

In recent years, growing interest in potential applications for three-dimensional (3-D) ultrasonography has led to rapid development of new 3-D acquisition techniques. Those using position and orientation measurement (POM) devices capable of tracking scanheads in six degrees-of–freedom (6-DOF) have received considerable attention, primarily due to their ease of use in the clinical setting as compared to mechanical tracking devices. Initial work on *in vitro* calibration and validation studies of this technology demonstrated that precise spatial location of fixed feature points can be accomplished using a 3-D ultrasound (US) imaging system based upon magnetic position and orientation measurement (Detmer et al. 1994). In further studies using a POM device, *in vitro* validation for volume measurements of a uniform latex phantom and for detection of luminal changes within stenotic vessel phantoms, as well as *in vivo* data on the clinical utility of this method for investigation of lower extremity vein grafts, were provided (Hodges et al. 1994). Using improved POM technology, it has been demonstrated that the rms uncertainty in point location can be less than 1 mm for typical US applications (Leotta et al. 1997). Because one of the key issues in 3-D ultrasonography using POM devices is accurate registration of US images to a regular 3-D volume, extensive work has been undertaken to achieve optimal calibration of 6-DOF systems (Barry et al. 1997; Prager et al. 1998). Recently, a sophisticated automated method for 6-DOF calibration has been presented (Rohling et al. 1998).

The primary advantage of using 6-DOF methods for 3-D US lies in the ability to register irregularly sampled US images obtained from different perspectives to a regular 3-D volume space; thus, potentially maximizing tissue information that may not be readily available from one imaging plane alone. Several investigations indicate that compounding these data would result in significant improvement in signal-to–noise ratio and speckle contrast (Barry et al. 1997; Hernandez et al. 1996; Hughes et al. 1996; Moskalik et al. 1995). Most reports on POM acquisition techniques, however, have limited their studies to volumetric scans or visualizations of various phantoms, organs or blood vessels using regular sampling

Address correspondence to: Stephen Meairs, M.D., Department of Neurology, University of Heidelberg, Klinikum Mannheim, D-68135 Mannheim, Germany. E-mail: meairs@neuro.ma.uni-heidelberg.de

(*i.e.*, acquisition of planar data as the transducer is moved along a single coordinate axis with avoidance of coincident image frames) (Hughes et al. 1996; Gilja et al. 1998; Kampmann et al. 1998), not exploiting the potentially useful feature of compounding data. Recently, a system for compounded registration of multiple 6-DOF US data sets has been described (Rohling et al. 1998). Through implementation of established techniques for multimodal image registration (*i.e.*, MRI and CT, PET and MRI), the authors convincingly demonstrated how multiple 3-D US volumes of a gall bladder, each of which were regularly sampled from a different imaging orientation, can be registered to a single volume. Their results provide further evidence that data compounding can significantly enhance the quality of volume reconstruction.

Reconstruction of irregular, arbitrary plane 6-DOF US data is highly complex. Because images are acquired in arbitrary orientation and position, it is often difficult to ascertain if the region-of–interest (ROI) has been completely scanned for volume reconstruction and visualization. This can lead to regions of missing data, which, to the dismay of the ultrasonographer, are readily displayed in volume renderings. If the US images are acquired roughly parallel and temporally successive slices are physically next to each other, then a missing space between successive slices can be easily interpolated in an incremental fashion. However, neither of these are true in the actual acquisition process using a "fully freehand" technique. Here, the acquired images are oblique and it is nearly impossible to define a "space between slices." If slices are far apart, then it is meaningless to interpolate all voxels between them with only the information from two US images. Because US reflection and backscatter intensities are angle-dependent (Picano et al. 1985), a further problem arises for handling of overlapping data obtained from different insonation angles. Because these data occupy nearly identical voxel coordinates, the question of which intensity best represents the tissue structure under investigation is crucial. The problem of volume reconstruction of irregular 6-DOF data, then, is not limited to insertion of accurately registered US data slices into a regular 3-D volume, but also encompasses the incremental interpolation of the space between the slices as well as the determination of individual voxel intensities for compounded data. We present an advanced 6-DOF US system using a POM device featuring accurate temporal and spatial registration of 3-D and 4-D US data, and a reconstruction technique based upon an ellipsoid Gaussian convolution kernel for handling arbitrary, irregularly sampled US data. We demonstrate the utility of this system for cerebrovascular applications of 3-D and 4-D imaging of the carotid arteries, as well as for 3-D reconstructions of intracranial blood vessels.

METHOD

Hardware and software

US imaging was performed with an ATL HDI-5000 (Advanced Technology Laboratories, Bothel, WA). For transcranial duplex studies, we used a 2-MHz sector scanner. Imaging of the carotid arteries (B-mode, color Doppler flow, and power Doppler) was performed with a 5–12 MHz dynamic range linear array transducer. Images were digitized in RGB PAL format at 25 frames/s using a RGB framegrabber (Meteor RGB, Matrox Electronic Systems, Quebec, Canada) on a 350-MHz dual processor Pentium II. Digitized images were stored in real-time to a high-speed, 10,000-rpm UW-SCSI hard disk using custom multithreaded software for Windows NT 4.0. Image processing was done on a silicon graphics high impact workstation equipped with 384 mb RAM. Volume rendering was achieved with custom software implementing a C++ visualization library (VGL 2.1, Volume Graphics GmbH, Heidelberg, Germany). All volumes were rendered with the high quality ScatterHQ algorithm of the VGL library for realistic, shadowed images of selected volume scenes.

POM device

For scanhead tracking we used an electromagnetic sensor (Ascension Technologies, Vermont, CO) providing position (x, y, z) and orientation (α, β, γ) information relative to a fixed point given by a magnetic field transmitter. The transmitter consists of three orthogonally polarized coils transmitting a DC field that is detected by the sensor to establish its position and orientation. This information is sent over a RS232 serial port at 144 Hz. The resolution of the electromagnetic sensor as given by the hardware manufacturer is: $err_{\text{trans}} = 0.127$ mm, $err_{\text{rot}} = 0.025°$ for translation and rotation errors, respectively, and $RMS_{\text{trans}} = 0.94$ mm and $RMS_{\text{rot}} = 0.189°$. The minimal detectable translation of the receiver is $\Delta\text{trans}_{\text{min}} = 0.0044'' = 0.112$ mm, and the minimal rotation angle is given by $\Delta\text{rot}_{\text{min}} = 0.022°$ equivalent to $\Delta\chi_{|r=\ 2\ \text{cm}} = 0.008$ mm and $\Delta\chi_{|r=\ 10\ \text{cm}} = 0.038$ mm.

ECG gating

ECG gating utilized an 8-bit PC-ISA card (MCC GmbH, Karlsruhe, Germany) connected to a serial port providing data on pulse rate, R-wave trigger and ECG curve for conventional Einthoven leads at a report rate of 150 Hz. Figure 1 shows a schematic drawing of the hardware components.

Data acquisition and synchronization

Each data component for 6-DOF acquisition (position orientation data, ECG R-waves and digitized image frames) was acquired in a separate thread of the software program.

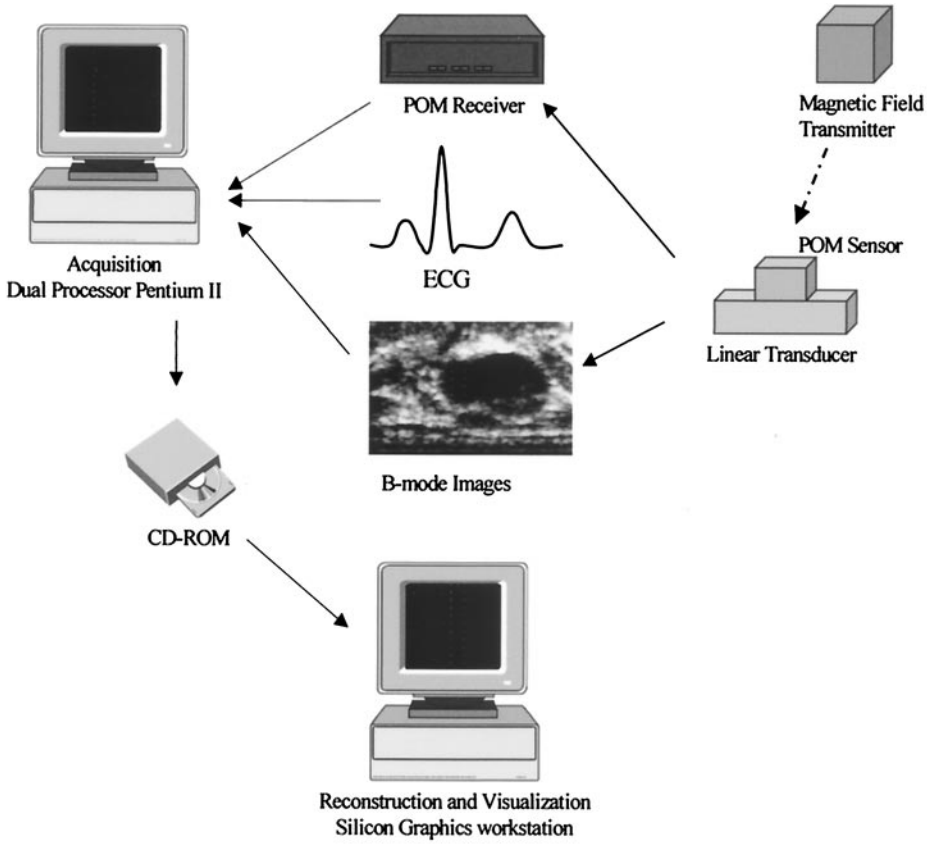

Fig. 1. Schematic illustration of hardware components composing scanhead tracking 6-DOF acquisition system. The POM sensor is attached to a linear transducer. The sensor sends information on the magnetic field emitted by the transmitter to the POM receiver, which decodes the field information for output of position and orientation data over a RS232 serial port at 144 Hz to a dual processor Pentium II computer. Images are digitized in PAL format at 25 frames/s using a RGB framegrabber. ECG gating is implemented with an 8-bit ISA card using the R-wave signal. With custom software using a multithreaded approach, each component is continuously streamed and assigned an internal clock value with a resolution of 200 μs. Raw data are archived on CD-ROM and postprocessed on a silicon graphics workstation for reconstruction and visualization using VGL.

This enabled data collection of a continuous stream output from the POM device, resulting in approximately six position measurements for each digitized image frame. The arrival of each POM data set, ECG R-wave and digitized image was time stamped at a clock resolution of 200 μs. Postprocessing of these time stamps enabled optimal synchronization of the three components for 3-D and 4-D volume reconstructions. It also allowed prompt recognition of possible frame drops. Threaded acquisition of the POM data enabled signal enhancement with a low-pass Fourier filter (Fig. 2). To account for discrepancies between actual US frame rate and the constant analog video frame rate of 25/s, we also acquired the coded information in each analog video frame on whether the image corresponded to a current US image frame or not. This information was kindly supplied by the manufacturer. Only those frames identified as current US images were used for volume reconstruction.

Prior to 3-D image acquisition, a full image was digitized for pixel calibration, determination of image zero-point (see below) and definition of a rectangular ROI. During continuous data acquisition, only the ROI was written to the hard disk, assuring that the actual data throughput over the PCI-bus did not exceed the maximal level specified by our hardware configuration. This data limit was ascertained by testing the ability of the system to acquire increasingly larger ROIs in real-time.

Sensor calibration

Prerequisite to calibration of the 6-DOF system is a validation of component timing. This assures that the system is capable of delivering position measurements that can be temporally assigned to a digitized image frame with a time shift within acceptable limits. Imaging was performed of the carotid artery with the transducer held steady for several s. Scanning was then abruptly interrupted by removing the transducer from the skin. The time stamp (in ms) of

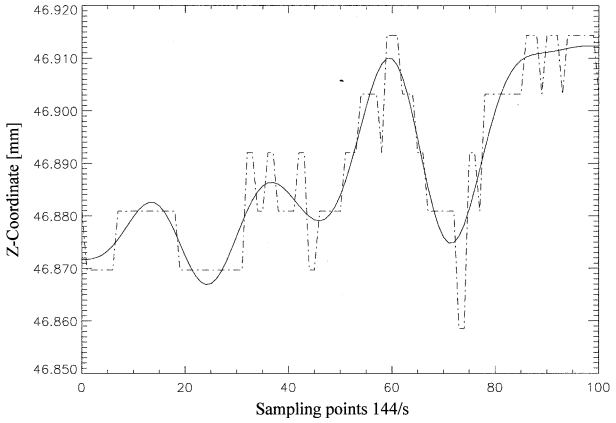

Fig. 2. Low-pass filtered fit of 100 sampling points (144/s) of z-axis rotational measurements reported by the electromagnetic sensor device (—·—·—).

the abrupt change in position measurements was compared to that of the acquired image data demonstrating the rapid transducer movement.

To determine inherent scaling and offsets of the 6-DOF system, we utilized a similar approach to calibration as that recently reported (Prager et al. 1998). Because the coordinate system (Fig. 3) of the 6-DOF position system is not identical to that of the generated US image, it is necessary to measure the offset $\vec{D} = (d_x, d_y, d_z)$ and the rotation angles α, β, and γ or, equivalently, the rotation matrix $\underline{\underline{T}} = \underline{\underline{T}}(\alpha, \beta, \gamma)$ for appropriate coordinate transformation.

The position $\vec{q} = (x", y", 0)$ of an image pixel is described in global coordinates $\vec{p} = (x, y, z)$ relative to the magnetic transmitter by a simple transformation:

$$\vec{p} = \vec{r} + \underline{\underline{M}}(\underline{\underline{C}}(\vec{p} + \vec{D})), \tag{1}$$

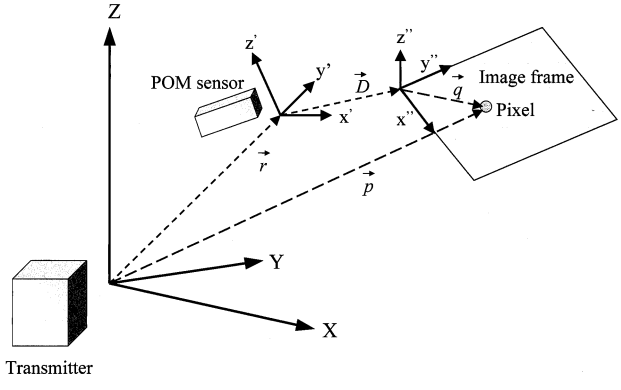

Fig. 3. Relationship between the coordinate systems of the magnetic field transmitter, position sensor and image frame.

where $\vec{r} = (x, y, z)$ is the measured distance between the transmitter and the sensor as reported in the current position and $\underline{\underline{M}} = \underline{\underline{M}}(\alpha, \beta, \gamma)$ is the rotation matrix transforming transmitter coordinates to the current sensor coordinate system.

The position of a pixel is defined by its distance $(x", y")$ from the zero point of the image frame, which, in turn, has an offset of $\vec{D}$ from the zero point of the magnetic sensor and is rotated against it using the matrix $\underline{\underline{C}} = \underline{\underline{C}}(\alpha_c, \beta_c, \gamma_c)$.

For calibration, the offset $\vec{D}$ and the rotation matrix $\underline{\underline{C}}$ are calculated:

$$\underline{\underline{C}}(\alpha,\beta,\gamma) = \begin{pmatrix} c_\beta c_\gamma & c_\gamma s_\alpha s_\beta - c_\alpha s_\gamma & c_\alpha c_\gamma s_\beta + s_\alpha s_\gamma \\ c_\beta c_\gamma & s_\alpha s_\beta s_\gamma + c_\alpha c_\gamma & c_\alpha s_\beta s_\gamma - c_\gamma s_\alpha \\ -s_\beta & c_\beta s_\alpha & c_\alpha c_\beta \end{pmatrix}, \tag{2}$$

where

$$c_\alpha = \cos(\alpha_c) \quad c_\beta = \cos(\beta_c) \quad c_\gamma = \cos(\gamma_c)$$
$$s_\alpha = \sin(\alpha_c) \quad s_\beta = \sin(\beta_c) \quad s_\gamma = \sin(\gamma_c). \tag{3}$$

If one acquires images that depict constant reference points using two or more measurements, it is possible to calculate the unknown parameters. One obtains, for the measurement n and point (pixel) i:

$$\vec{p}_i^{\,n} = \vec{r}^{\,n} + \underline{\underline{M}}^n(\underline{\underline{C}}(\vec{q}_i^{\,n} + \vec{D})), \tag{4}$$

together with measurement m and pixel j describing the same global coordinates as pixel i:

$$\vec{p}_i^{\,n} - \vec{p}_j^{\,m} = \vec{0}. \tag{5}$$

A simple phantom was constructed for calibration of the 6-DOF sensor system. Small bore holes were drilled into the sides of a rectangular plastic container to accommodate thin, 0.15-mm gauge nylon wires for construction of a triangle, subtended by approximately 60° angles along the transverse plane of the container as defined by the points of intersection of the nylon wires. The sides of the triangle measured maximally 3 cm. This distance was chosen to allow adequate visualization of any two points of the triangle with the transducers we used in these experiments. Two additional wires of the same caliber were crossed perpendicularly to form an intersection centered at 2 cm below the triangle. It should be noted that the calibration algorithms do not require *a priori* knowledge of distances or angles between the points to be evaluated and are based strictly on proper identification of each crossover point of two wires in the calibration images.

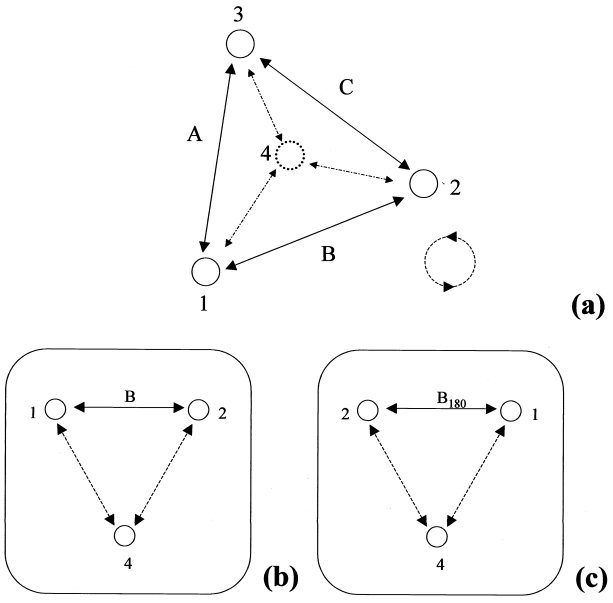

Fig. 4. Schematic illustration of 6-DOF sensor calibration. (a) Circles 1–3 represent the intersections of thin-gauge wires along one plane in the calibration box. Circle 4 represents the intersection of two wires approximately 2 cm below the other three intersections. Calibration is performed by systematic digitization of B-mode images with corresponding POM data from three viewpoints (A–C), each of which views two intersections in the top calibration plane and the crossed wire intersection (circle 4). (b) The result is shown for imaging of the intersections 1 and 2. (c) The transducer is then rotated 180°.

Calibration of digitized US images to the position sensor system requires the definition of an image zero point. For a linear transducer image, this is the center of the first scan line and, in a sector image, this is represented by the tip of the sector nearest the transducer. The pixel resolution of the image is obtained by measuring the number of pixels between two image depth calipers of known distance.

Calibration involved the acquisition of a series of images in the water-filled calibration box at 37° C, each of which visualized three of the four wire intersections along one plane (Figs. 4 and 5). Acquisition was performed in a systematic manner, with scanning of the tetrahedra along each nonhorizontal plane, with additional 180° rotation of the scanhead, resulting in a total of six images for each calibration series. Low-pass filtering of the position and orientation data was done for 50 measurements before and immediately following the digitization of each calibration image.

Determination of the image coordinates of the four wire intersections of the phantom from different imaging planes and positions enabled the calibration parameters $\vec{D}$ and $\underline{\underline{C}}$ to be calculated numerically using a Levenberg–Marquardt nonlinear least-squared fit.

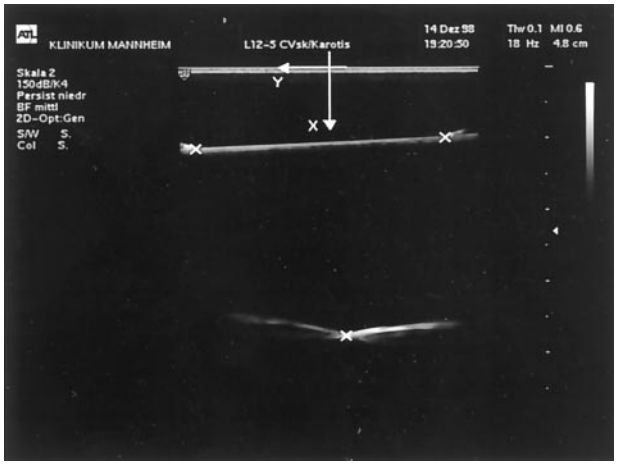

Fig. 5. Calibration image for linear array. The image zero point is represented by intersection of arrows denoting x and y coordinate axes. Depth calipers on the right are used for calibration of pixel resolution. The three wire intersections (marked by ×) are used to calibrate the POM device.

Volume reconstruction

The first step in volume reconstruction of irregularly sampled US data is definition of a global regular volume, the extents of which are derived from the actual POM data and the size of the ROI. Registration of an image frame to this regular volume is performed by using the corresponding low-pass filtered POM data to translate and rotate each of its pixels using (x'', y'') offsets. This process can be described as:

$$V(\vec{x}) = \sum_{n=0}^{N} \widehat{T}^n \cdot I^n(\vec{q}); \quad q = \begin{pmatrix} x'' \\ y'' \\ 0 \end{pmatrix}, \quad x = \begin{pmatrix} x \\ y \\ z \end{pmatrix}, \tag{6}$$

where $I^n(\vec{q})$ is the pixel intensity at the image coordinate $\vec{q}$ of image n, $V(\vec{x})$ is the reconstructed voxel value at $\vec{x}$, N is the number of images, and $\widehat{T}^n = \widehat{T}^n(\vec{r}^n, \underline{\underline{M}}^n)$ is the operator depending on frame offset $\vec{r}^n$ and rotation matrix $\underline{\underline{M}}^n = \underline{\underline{M}}(\alpha^n, \beta^n, \gamma^n)$ transforming from image to global coordinates:

$$\widehat{T} \cdot f(\vec{x}') := f(\underline{\underline{T}} \cdot \vec{x}') = f(\vec{r}\underline{\underline{M}}\vec{x}') = f(\vec{x}). \tag{7}$$

If $\vec{q}$ (0, 0, 0) is not at the center of rotation, it is necessary to add the calibration offset $\vec{D}$ and the rotation matrix $\underline{\underline{C}}$, eqn (4), leading to:

$$\widehat{T} \cdot f(\vec{q}) := f(\underline{\underline{T}} \cdot \vec{q}) = f(\vec{r} + \underline{\underline{M}}(\underline{\underline{C}}\vec{q} + \vec{D})) = f(\vec{x}). \tag{8}$$

To deal with arbitrary irregularly sampled US data, we first place a Gauss convolution kernel around each

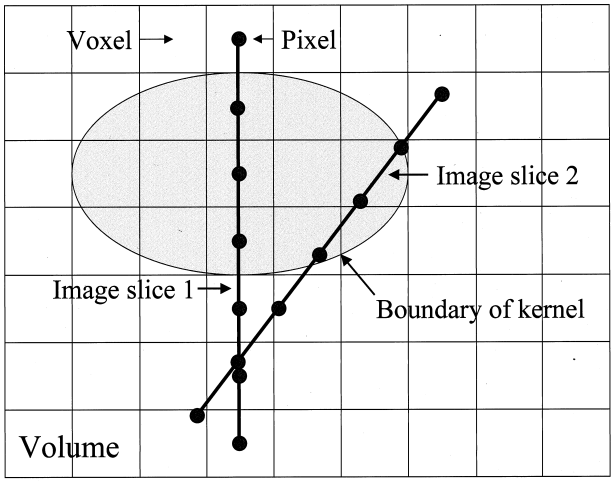

Fig. 6. Volume reconstruction using an ellipsoid convolution kernel. Two images, taken from different angles along the same imaging plane are registered to the 3-D volume. Image pixels are represented by ●. The value of an individual voxel intensity is calculated by placing the convolution kernel (ellipse) around this voxel and weighting the contribution of other voxel intensities within the kernel according to their distance from the center of the 3-D ellipsoid.

voxel during insertion of the image into the regular 3-D volume:

$$V(\vec{x}) = \frac{\sum_{n=0}^{N} \sum_{\vec{x}'} \widehat{G}_{k,s} \cdot \widehat{T}^n \cdot I^n(\vec{q}) \delta_{\vec{x}-\vec{x}'}}{\sum_{n=0}^{N} \sum_{\vec{x}'} \widehat{G}_{k,s} \cdot \vec{1} \delta_{\vec{x}-\vec{x}'}}, \quad (9)$$

where $\widehat{G}_{k,s}$ is the Gauss convolution operator of kernel size k acting on a function $f(\vec{x})$ as:

$$\widehat{G}_{k,s} \cdot f(\vec{x}) = \sum_{\vec{k}'=0}^{\vec{k}} f(\vec{x}) e^{-\frac{(\vec{k}')^2}{s}}, \ \vec{k} = (k_x, k_y, k_z), \quad (10)$$

and fwhm (full-width-half-maximum) s.

Each pixel value $I(\vec{q})$ is transformed into volume coordinates and is surrounded with a 3-D Gauss sphere of the same intensity value. Using $\widehat{G}_{k,s} \cdot \vec{1}$ as weight function and dividing after completed insertion into the 3-D volume, eqn (9), leads to a voxel value composed as the weighted sum of all transformed pixel intensities in the neighborhood defined by the kernel size k. Because smoothing of image data in the horizontal direction may not be desirable over more than the next neighboring voxels, we do not use spherical kernels but, rather, ellipsoid kernels whose main axis is orientated along the frame normal of the current image plane using an exponential weight according to the distance from the estimated voxel location (Fig. 6).

Using $\vec{n}''_q = (0, 0, 1)$ as normal to the image plane in the (x'', y'', z'') system, we get

$$\vec{n}_q = \underline{\underline{M}}\, \underline{\underline{C}} \vec{n}''_q \quad (11)$$

in volume coordinates. Weighting the ellipsoid with a factor F, one obtains:

$$\widehat{G}_{k,s,F} \cdot f(\vec{x}) = \sum_{\vec{k}'=0}^{\vec{k}} f(\vec{x}) e^{\left[-\frac{(\vec{k}')^2}{s}\left(1-F\frac{\vec{n}_q\vec{k}'}{|\vec{k}|}\right)\right]}, \quad F \geq 0. \quad (12)$$

Extending these algorithms to 4-D US acquisition, we obtain, for the discrete time domain $n \rightarrow n_t$ $(N \rightarrow N_t)$ and, for the volume data, $V(\vec{x}) \rightarrow V_t(\vec{x})$.

RESULTS

Time delay between POM data and digitized ultrasound images

Twenty measurements of time delay between arrival of position data and image acquisition were performed. Maximum time delay of 25.1 ms (mean 17.6 ms, SD ± 5.0 ms) between the two data acquisitions is below the frame period (40 ms); thus, validating the system for acceptable temporal synchronization. A delay of position data following the image acquisition was not observed.

Real-time data archiving

At an image ROI of 256 × 256 pixels there was no loss of frames (25 fps) in the RGB raw data files over a scan time of 3 min. Due to the maximum hard disk performance of about 7 MB/s, frame rate dropped to 24 fps at an ROI of 300 × 300 pixels and to 16 fps at an ROI of 384 × 384 pixels for RGB (24-bit) data.

6-DOF calibration

The Levenberg–Marquardt algorithm converged to a stable solution for all calibrations in 4 to 6 iterations. Parameters for calibration were well identified in all images, resulting in a sufficient range of angles to establish a well-conditioned problem. The quality and precision of the calibration algorithms were assessed by established procedures (Prager et al. 1998). Although not directly comparable, the results of these measurements (Tables 1 and 2) are presented, together with those of the Cambridge and the three-wire calibration methods (Prager et al. 1998).

3-D B-mode imaging of the carotid artery

An important goal in cerebrovascular 3-D US research is to improve reconstructions of carotid arteries to

Table 1. Quality of calibration

	Mannheim	Cambridge	Three-wire
Observations	120	190	45
Mean value (mm)	1.81	0.92	5.37
Maximum value (mm)	8.69	2.32	10.09
Standard deviation	1.3	–	–

Difference of the position of one point in the us image (Mannheim: 2 cm left of center and 3.5 cm depth) for different calibrations in reference to the magnetic sensor (16 calibrations) (Prager et al. 1998).

allow better evaluation of atherosclerotic disease. Figure 7 illustrates the excellent detail of arterial wall structure that can be obtained upon visualization of a 3-D reconstruction of irregularly sampled B-mode images from the carotid artery.

3-D power Doppler imaging of high-grade carotid stenosis

Due to its relatively angle-independent characteristics and superior ability to delineate blood vessel walls and atherosclerotic plaques (Steinke et al. 1996), power Doppler imaging is a promising technique for 3-D ultrasonography of the carotid arteries using compounded, irregularly sampled image data. Figure 8 demonstrates a volume-rendered image of a high-grade stenosis of the internal carotid artery (maximal velocity 420 cm/s) reconstructed from ECG-gated power Doppler images acquired in an irregularly sampled fashion.

Internal skull surface

3-D visualization of the internal skull surface can be useful for demonstrating the angular limits of insonation through a temporal bone window. Such information may be valuable, for example, in assessment of the ability of transcranial contrast-enhanced duplex sonography to depict thrombosis of the transverse sinus. If the skull surface in the region of this vein cannot be reconstructed and visualized, a negative study cannot be taken as definitive evidence of venous thrombosis. The same

Table 2. Calibration precision

	Mannheim	Cambridge	Three-wire
Observations	15,840	25,320	25,320
Mean value (mm)	2.11	2.17	1.65
Maximum value (mm)	6.01	7.13	4.78
Standard deviation	1.78	–	–

Size of cloud of points due to the reconstruction of one point (one crossing of wires) from 45 views/16 calibrations (x = ± 27.5 cm; y = ± 22 cm; z = ± 8 cm; angle = 60°; twist = ± 89°) (Prager et al. 1998).

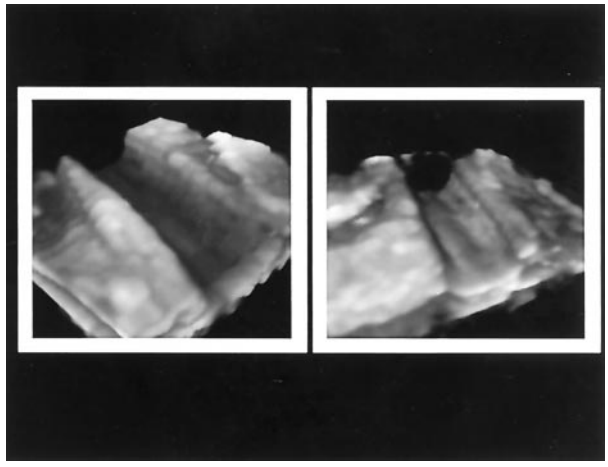

Fig. 7. Two views of a reconstruction of the carotid artery from 3-D 6-DOF US data, acquired with irregular sampling. Half of the vessel is opened up to accomodate visualization. Note the excellent depiction of the arterial wall surface.

holds true for visualization of the superior sagittal sinus, which, in contrast to the transverse sinus, is rarely accessible with contrast-enhanced ultrasonography. Volume rendering of the skull surface in Fig. 9 was obtained from 6-DOF transcranial B-mode imaging through the contralateral temporal bone window. Volume reconstruction was performed from multiple arbitrary plane data.

4-D color flow Doppler imaging of the carotid bifurcation

For a typical 4-D color Doppler flow scan of the carotid bifurcation, approximately 6000 images are acquired. Because the 6-DOF system uses RGB data acquisition, separation of color-flow Doppler signals from grey-scale B-mode signals is relatively straightforward. This allows construction of two 4-D data sets consisting of 8-bit grey-scale and 24-bit color volumes (number of volumes = fps/beats per s). Because the B-mode and color Doppler images have identical coordinate systems, reconstruction is performed in a parallel fashion for each temporal volume frame. This typically results in two sets of 16 to 22 reconstructed volumes, depending on heart rate. Simultaneous volume rendering of B-mode and color Doppler volumes at a specified time offset from the ECG R-wave is accomplished with the visualization library, VGL. Through use of different transparencies and opacities for the two individual volumes, it is possible to obtain optimal visualization of 4-D color flow imaging with concurrent display of the B-mode reconstruction of the arterial walls and surrounding tissue (Fig. 10). As opposed to other applications using only B-mode or power Doppler imaging, the data is not irregularly sampled, being roughly parallel to the longitudinal axis of the

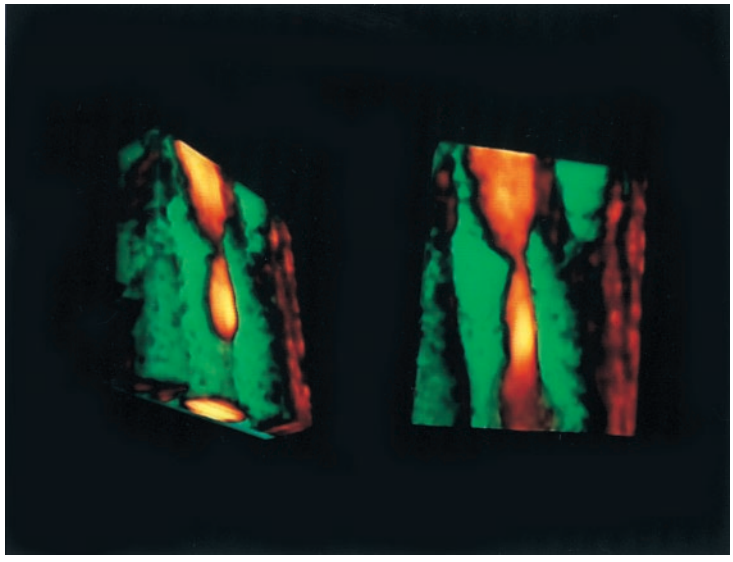

Fig. 8. Volume rendering of high-grade carotid stenosis. Data were acquired with 6-DOF scanhead tracking. Irregularly sampled power Doppler images served as raw data for the reconstruction. Note the excellent definition of stenosis and the surrounding weakly echogenic plaque material, color-coded in green. The vessel walls of the carotid artery are well delineated.

arteries. This restriction is due to the inherent qualities of color Doppler, which color-codes the direction of blood flow velocity relative to the transducer orientation. Variations in the Doppler angle also affect the Doppler shift and, hence, the precise color displayed.

DISCUSSION

Information on 3-D reconstruction of irregularly sampled arbitrary US data registered with a POM device is limited. One group addressing this problem has proposed calculation of individual voxel intensities through distance-weighted averaging of the sum of pixels registered within the voxel radius (Barry et al. 1997). Because the effect of pixels on neighboring voxels is not considered in this technique, reconstruction may result in significant discontinuities among gradient vectors from voxel to voxel that are quite visible on rendered images. We have attempted to overcome this limitation by introducing an ellipsoid Gaussian convolution kernel for handling arbitrary irregularly sampled US data. Because the Gauss kernel extends the image data in three dimensions, signal-to–noise ratio is not only reduced on the horizontal plane, but also on the vertical plane orthogonal to the current image plane. Use of an ellipsoid Gaussian convolution kernel may also partially compensate for the difficulty in representing the US beam thickness when inserting planar image data into the reconstructed volume.

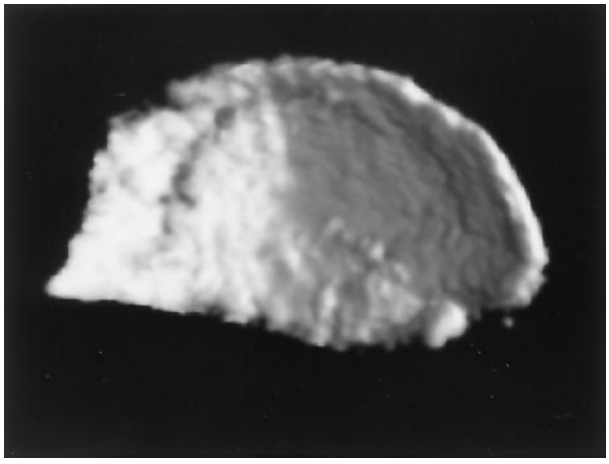

Fig. 9. Volume rendering of the skull surface. Data was acquired with 6-DOF transcranial B-mode imaging through the contralateral temporal bone window. Note the fine detail of the reconstructed bone.

Assessment of the quality of a particular reconstruction technique, especially in quantitative terms, is difficult. An interesting approach has been proposed that compares grid-mapped, high-intensity sampled data acquired with multiple angles of insonation to a single 2-D image using a novel measure of coherence, defined as the number of pixels identified in an interface boundary and the variation of the pixel intensity along this boundary (Barry et al. 1997). Although results using this technique impressively demonstrate a higher coherence for compounded US data (Barry et al. 1997), questions remain regarding the general applicability and validity of a specific segmentation algorithm for evaluation of reconstruction performance.

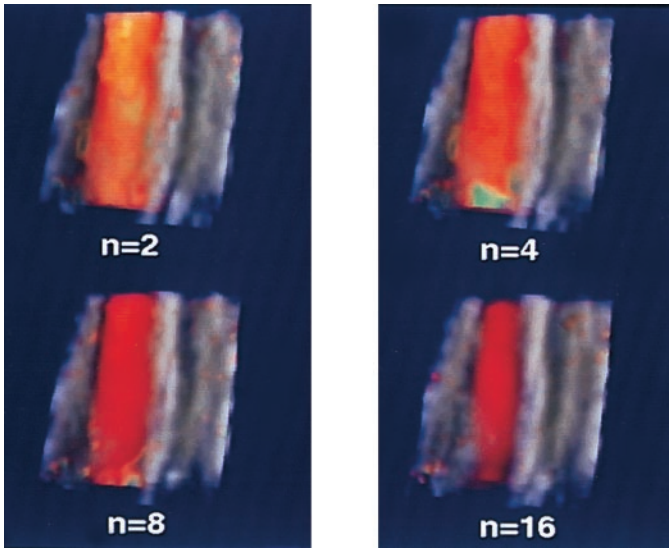

Fig. 10. 4-D color-flow imaging of the internal carotid artery with concurrent display of the B-mode reconstruction of the arterial walls and surrounding tissue. Four rendered volume frames from a total of 18 volumes during the cardiac cycle are displayed according to their relationship to the R-wave trigger (*i.e.,* onset of systole). Note the changes in color Doppler depicting higher mean velocities in systole. Also note the changes in arterial diameter as shown by the grey-scale renderings of the B-mode US data. Approximately 6000 images were acquired for this study. Rendering was performed with the Graphics Visual Library® on a silicon gGraphics high impact workstation.

One of the best ways to judge the quality of 3-D US volume acquisition and reconstruction is through volume visualization using rendering techniques. Although admittedly subjective, volume rendering can readily depict missing or improperly registered data: what you see is what you get. This method is particularly important for evaluation of irregularly sampled, 3-D US data. Errors in calibration, faulty reconstruction techniques, motion artefacts and temporal mismatches of position and orientation information will be efficiently displayed with volume rendering. Indeed, visualization is a prerequisite to quantitative 3-D ultrasonographic analysis: volumetric calculations or segmentations of 3-D US data that cannot be adequately rendered can be hazardous tasks. Most importantly, however, the quality of 3-D volume renderings in cerebrovascular applications will be judged according to the ability of the rendered images to depict vascular pathology as compared to established techniques such as magnetic resonance angiography. This will ultimately determine whether this new 3-D US technology will assume a firm role in routine clinical practice. For these reasons, we have presented our results primarily in the form of volume renderings of actual patient data to depict the value of the investigated acquisition and reconstruction techniques. The results, although restricted to the field of cerebrovascular disease, may be of value to other applications of 3-D sonography, particularly those in which compounding of data through irregular sampling may provide superior information on tissue or vessel structure. To our knowledge, these renderings are the first *in vivo* examples of volume rendering of irregularly sampled US data using a 6-DOF scanhead tracking system to appear in the literature.

Applications that exploit the benefits of compounded data with arbitrary image sampling require acquisition of large data sets. This is particularly true for 4-D ultrasonography of the carotid arteries, for example, where over 6000 ECG-gated images are required for adequate volume reconstructions. Our results on real-time data archiving demonstrate that, by using custom, multithreaded software on a dual-processor computer, very large US data sets of sufficient image dimensions for 3-D volume reconstructions can be acquired directly to a hard disk without data compression. Thus, the total size of the raw data is limited only by hard disk capacity. The advantage of this technique is that it overcomes the restrictions on maximum data size when using only RAM memory for image acquisition, a method that has been used in virtually all 3-D US systems previously described in the literature. The only exception to this rule has been a novel method for data archiving to S-VHS video tapes with simultaneous recording of POM information on the audio channel (Barry et al. 1997). Other than a loss of image quality through redigitization of individual video frames, this technique is limited by its strictly off-line approach without potential application to real-time visualization, an area of research that is currently receiving keen attention.

For assessment of the critical issues of POM calibration quality and precision, we used established techniques (Prager et al. 1998). Our results compare favorably to those

reported for the cross-wire technique and Cambridge phantom (Prager et al. 1998). Due to its rapid automatic calibration capabilities, however, the Cambridge phantom appears to offer distinct advantages for clinical applications requiring repeated calibration of 6-DOF devices.

A significant problem, not previously addressed in the literature, is that of discrepancy between actual US image frame rate (depending on transducer frequency, pulse repetition rate, depth, persistence, etc) and the fixed analog (PAL, NTSC or SECAM) frame rate of digitized images. Information on analog conversion is generally not available from the US manufacturer, and it appears that each company has it own proprietary technique for dealing with analog output. As the discrepancy between image frame rate and that of the analog output increases, the number of digitized frames with duplicate or interpolated image information also increases. At low frame rates, occurring, for example, in transcranial applications using power Doppler imaging, this can result in a significant mismatch between the actual image coordinates of "duplicate" frames digitized from an analog video source and those of updated POM measurements, especially when the POM device is reporting significant transducer motion at the time of image digitization. Fortunately, on the HDI 5000 from ATL, each analog video frame possesses coded data on whether it corresponds to a current US image frame or not. The method for decoding this information was kindly provided by the manufacturer and allowed us to sort out the analog RGB signals to achieve registration of pertinent US image data at the actual US frame rate. This approach using only relevant US data (within the maximal PAL timing error approaching 25 ms) contributes to improved volume reconstruction in our application.

One weakness in our POM system is that of digital image acquisition. Although we have implemented the best available analog format (RGB), the image quality remains inferior to that of the original digital US images. Moreover, the application is confronted with the task of sorting out pertinent US data when frame rates are below that of the analog output. Frame rates in excess of the PAL standard of 25/s (or NTSC 30/s) cannot be fully captured. An ideal solution to this problem would be synchronization of the manufacturer's digital images with image position and orientation measurements; thus, alleviating the need to digitize analog data. This promising technique is currently in development.

CONCLUSIONS AND FUTURE WORK

This study describes new approaches to 3-D and 4-D US image acquisition and volume reconstruction. It demonstrates how real-time data archiving using multithreaded software and dual-processor hardware can overcome the limitations imposed by RAM memory techniques, thereby allowing adequate data acquisition for compounded reconstructions, as well as for applications such as 4-D color Doppler flow imaging. Optimization of 3-D volume reconstruction of irregularly sampled US data registered by a POM system can be achieved with an ellipsoid convolution algorithm using exponential weighting. The utility of this approach has been demonstrated using sophisticated volume rendering techniques on reconstructed *in vivo* US data sets.

Future work will concentrate on clinical appraisal of 3-D and 4-D renderings of compounded ultrasonographic data in a number of promising cerebrovascular applications. These include 4-D carotid plaque motion analysis, characterization of vessel wall motion in early atherosclerosis, assessment of extra- and intracranial stenosis, and quantitative 4-D color Doppler flow imaging.

Acknowledgements—This work was supported by the Forschungsfond Klima 97/98 and BMH4-CT98-3782. We thank Advanced Technology Laboratories for their kind assistance in providing us with detailed information regarding decoding of their analog video output.

REFERENCES

Barry CD, Allott CP, John NW, Mellor PM, Arundel PA, Thomson DS, Waterton JC. Three-dimensional freehand ultrasound: image reconstruction and volume analysis. Ultrasound Med Biol 1997;23:1209–1224.

Detmer PR, Bashein G, Hodges T, Beach KW, Filer EP, Burns DH, Strandness DEJ. 3-D ultrasonic image feature localization based on magnetic scanhead tracking: in vitro calibration and validation. Ultrasound Med Biol 1994;20:923–936.

Gilja OH, Hausken T, Olafsson S, Matre K, Odegaard S. In vitro evaluation of three-dimensional ultrasonography based on magnetic scanhead tracking. Ultrasound Med Biol 1998;24:1161–1167.

Hernandez A, Basset O, Chirossel P, Gimenez G. Spatial compounding in ultrasound imaging using an articulated scan arm. Ultrasound Med Biol 1996;22:229–238.

Hodges TC, Detmer PR, Burns DH, Beach KW, Strandness DEJ. Ultrasonic three-dimensional reconstruction: in vitro and in vivo volume and area measurement. Ultrasound Med Biol 1994;20:719–729.

Hughes SW, D'Arcy TJ, Maxwell DJ, Chiu W, Milner A, Saunders JE, Sheppard RJ. Volume estimation from multiplanar 2D ultrasound images using a remote electromagnetic position and orientation sensor. Ultrasound Med Biol 1996;22:561–572.

Kampmann W, Walka MM, Vogel M, Obladen M. 3-D sonographic volume measurement of the cerebral ventricular system: in vitro validation. Ultrasound Med Biol 1998;24:1169–1174.

Leotta DF, Detmer PR, Martin RW. Performance of a miniature magnetic position sensor for three-dimensional ultrasound imaging. Ultrasound Med Biol 1997;23:597–609.

Moskalik A, Carson PL, Meyer CR, Fowlkes JB, Rubin JM, Roubidoux MA. Registration of three-dimensional compound ultrasound scans of the breast for refraction and motion correction. Ultrasound Med Biol 1995;21:769–778.

Picano E, Landini L, Distante A, Salvadori M, Lattanzi F. Angle dependence of ultrasonic backscatter in arterial tissues; a study in vitro. Circulation 1985;72:573–576.

Prager RW, Rohling RN, Gee AH, Berman L. Rapid calibration of 3-D freehand ultrasound. Ultrasound Med Biol 1998;24:855–869.

Rohling RN, Gee AH, Berman L. Automatic registration of 3-D ultrasound images. Ultrasound Med Biol 1998;24:841–854.

Steinke W, Meairs S, Ries S, Hennerici M. Sonographic assessment of carotid artery stenosis: comparison of power Doppler imaging and color Doppler flow imaging. Stroke 1996;27:91–94.